Title	A C0 zig-zag model for the analysis of angle-ply composite thick plates
Author(s)	Wu, Z; Lo, SH; Ren, XH
Citation	Composite Structures, 2015, v. 127, p. 211-223
Issued Date	2015
URL	http://hdl.handle.net/10722/250260
Rights	This work is licensed under a Creative Commons Attribution-NonCommercial-NoDerivatives 4.0 International License.

A C^0 zig-zag model for the analysis of angle-ply composite thick plates

Wu Zhen[1,2], S. H. Lo[3*], Ren Xiaohui[1,2]

[1]*Key Laboratory of Liaoning Province for Composite Structural Analysis of Aerocraft and Simulation, Shenyang Aerospace University, Shenyang 110136, China*

[2]*College of Aerospace Engineering, Chongqing University, Chongqing 400040. China*

[3]*Department of Civil Engineering, University of Hong Kong, Pokfulam Road, Hong Kong, China*

Abstract: From a theoretical and practical viewpoint, the zig-zag theory is well adopted in the analysis of laminated composite structures. Nevertheless, for the available zig-zag models, artificial constraints in which the first derivatives of transverse displacement are replaced by the assumed variables have to be employed to avoid C^1 interpolation functions in the finite element implementation. Such artificial constraints violate continuity conditions of interlaminar transverse stresses at interfaces. To avoid using artificial constraints, a C^0-type zig-zag model is proposed in this paper. C^0 interpolation functions are only required in the finite element formulation as first derivatives of transverse displacement have all been eliminated from the displacement field based on stress compatibility conditions between plies and on the top and bottom surfaces of the plate. Moreover, the number of variables involved in the proposed zig-zag model is less than that of the existing zig-zag models, yet accurate results are produced comparable to analytical solutions and three-dimensional finite element results. Effects of ply orientations, boundary conditions and length-to-thickness ratio on displacements and stresses of laminated composite plates have been studied.

Keywords: C^0 zig-zag theory; Composite plates; Angle-ply; Finite element formulation

1. Introduction

Laminated composite structures are frequently applied in aerospace, automotive and civil engineering due to their advantages of high stiffness, high strength and low

* Corresponding author. Tel.: +852 28591977.

† E-mail address: hreclsh@ hku.hk (S.H. Lo)

weight. In order to achieve an effective design, the mechanical behaviors of multilayered composite structures ought to be assessed as accurate as possible. However, the analysis and the design of laminated composite structures are more challenging compared with conventional one-layer metallic structures as the material is weak in shear compared to extensional rigidity. Thus, transverse shear deformation of laminated composite structures has to be rigorously modeled. In addition, Carrera [1] showed that the in-plane displacement field for multilayered composite structures exhibits discontinuous derivatives with respect to each interface which is known as zig-zag effect.

In order to model the variation of the zig-zag form of in-plane displacement components along the thickness direction, Murakami [2] developed a zig-zag theory by adding a zigzag-shaped function (ZZF) to the in-plane displacement filed of the global displacement. By adding the zig-zag shape function in Legendre polynomials, Toledano and Murakami [3] proposed an improved zig-zag theory. By analyzing the cylindrical bending problems of laminated plates, it is found that the proposed zig-zag theory is able to improve the accuracy of in-plane displacements and stresses. By adding the ZZF to displacement field, Brischetto et al. [4] proposed a higher-order model for bending analysis of sandwich plates. Numerical investigation showed that accuracy of both displacement and stress evaluations can be significantly improved by using the ZZF. Carrera [5] employed the Murakami's zig-zag theory to study the bending problems of laminated composite plates and shells. Numerical results show that the introduction of zig-zag function is more effective than increasing the order of the global displacement. In addition, Rodrigues et al. [6] employed the Murakami's zig-zag theory for the static, vibration and buckling analysis of laminated composite plates. Neves et al. [7] extended the Murakami's zig-zag theory for the analysis of functionally graded plates.

The advantages of using the Murakami's zig-zag theory to analyze the laminated composite plates have been studied by Rodrigues et al. [8]. However, Murakami’s zig-zag model violated the interlaminar continuity for the transverse stresses. Dafedar et al. [9] showed that the higher-order model violating continuity conditions of interlaminar stresses overestimates the critical loads of soft core sandwich plates. As a result, zig-zag models [10-15] were developed that take into account the zig-zag effect and interlaminar continuity for transverse stresses in multilayered composite structures. However, constitutive equations in these zig-zag models are based on the plane stress assumption, in which transverse shear deformation effect is only included

but transverse normal deformation has been neglected. For thermo-mechanical problems of moderate thick composite plates, transverse normal deformation ought to be considered as transverse normal deformation is equally important compared to in-plane deformations [16,17]. By taking into account transverse normal strain, Cho and Oh [18] proposed a higher order zig-zag model to predict the deformation and stresses of thick smart composite plate subjected to mechanical, thermal and electric loads. In their model, the second derivatives of transverse displacement components have been involved in the expression of strain energy. Therefore, C^1 interpolation functions are required in the finite element implementation. In order to circumvent the requirement of C^1 continuity, Oh and Cho [19] employed the thin plate non-conforming triangular element proposed by Specht [20] which can only satisfy C^1 continuity condition at the nodes. For the zig-zag model, the transverse shear stresses are unable to be obtained directly from the constitutive equations. In order to evaluate transverse shear stresses, stress smoothing technique within the entire domain has been adopted in regular meshes. An historical review on the zig-zag theories can be found in reference [21].

To avoid using the C^1 continuity displacement functions in zig-zag model's finite element implementation, Pandit et al. [22] employed some artificial constraints in which the first derivatives of transverse displacement are replaced by the assumed variables. The same technique has been extended to analyze the vibration of sandwich plates with random material properties [23] and stochastic free vibration of soft-core sandwich plates [24]. By using the method of artificial constraints, Singh and Chakrabarti [25] proposed a C^0 finite element model based on the zig-zag theory to study the buckling of laminated composite plates. Khandelwal et al [26] also employed the assumed variables to replace the first derivatives of transverse displacement in the zig-zag model. Recently, Kumar et al. [27] studied the static problems of laminated composite and sandwich shells by a C^0 finite element formulation based on a higher-order zig-zag model using method of artificial constraints. However, numerical investigations show that such assumption will violate the continuity conditions of transverse shear stresses at interfaces.

In order to avoid the use of the C^1 interpolation functions and the artificial constraints in finite element implementation of the zig-zag theories, Ren et al. [28] proposed a zig-zag theory in which the first derivatives of transverse displacement have been suppressed from the displacement field of the zig-zag model. The C^0 interpolation functions are only needed in the finite element implementation. Without

the use of any artificial constraints, an six-node triangular element is developed for the static analysis of laminated composite and sandwich plates. Recently, by considering transverse normal strain, Wu et al. [29] proposed a C^0-type zig-zag model in which derivatives of transverse displacements are eliminated from the displacement field for static analysis of thick cross-ply composite beams. Numerical investigations showed that the C^0 zig-zag model [29] is more accurate than the C^1-type zig-zag model [18]. Moreover, the effects of displacement variables in zig-zag models on displacements and stresses have been studied. In order to develop a coherent model for the angle-ply laminated plates [30,31], the laminated composite structures have to be fully exploited. This paper proposes a C^0-type zig-zag model for thick laminated composite plates with general ply configurations. In addition to considering transverse normal strain, the merit of the proposed model is that derivatives of transverse displacement have been eliminated from the displacement field based on stress compatibility without artificial constraints. A six-node triangular element of the proposed C^0 zig-zag model is presented to study the angle-ply laminated composite plates with different geometries, boundary conditions and loadings. Numerical results show that the accuracy of existing zig-zag model rapidly deteriorates as the thickness of laminated plates increases. Boundary conditions also have great impact on the accuracy of the C^1-type zig-zag models; however, the proposed C^0-type model is able to produce promising results in all these circumstances.

2. Higher-order zig-zag model for thick angle-ply composite plates (ZZTC-C0)

In terms of the Cartesian coordinate system *x*, *y* and *z* on the middle plane of the rectangular plate *a*×*b* shown in Figure 1, an initial displacement field of the higher-order zig-zag model is expressed as

$$\begin{aligned} u^k(x,y,z) &= u_0(x,y) + \sum_{i=1}^{3} z^i u_i(x,y) + \sum_{i=1}^{k-1} S_x^i \left(z - z_i\right) H\left(z - z_i\right) \\ v^k(x,y,z) &= v_0(x,y) + \sum_{i=1}^{3} z^i v_i(x,y) + \sum_{i=1}^{k-1} S_y^i \left(z - z_i\right) H\left(z - z_i\right) \\ w^k\left(x,y,z\right) &= w_0\left(x,y\right) + z w_1(x,y) \end{aligned} \tag{1}$$

where the superscript *k* denotes the layer order of laminated plate, $H\left(z-z_i\right)$ is the Heaviside unit step function, S_x^i and S_y^i are the slopes of *i*th layer [26]. The

number of unknowns can be reduced by imposing the top and the bottom surface transverse shear free conditions and the transverse shear stress continuity conditions at interfaces.

The stress-strain relationships for a lamina with reference to the axis system (*x*, *y*, *z*) can be written as

$$\begin{Bmatrix} \sigma_x \\ \sigma_y \\ \sigma_z \\ \tau_{xz} \\ \tau_{yz} \\ \tau_{xy} \end{Bmatrix}^k = \begin{bmatrix} \bar{Q}_{11} & \bar{Q}_{12} & \bar{Q}_{13} & 0 & 0 & \bar{Q}_{16} \\ \bar{Q}_{21} & \bar{Q}_{22} & \bar{Q}_{23} & 0 & 0 & \bar{Q}_{26} \\ \bar{Q}_{31} & \bar{Q}_{32} & \bar{Q}_{33} & 0 & 0 & \bar{Q}_{36} \\ 0 & 0 & 0 & \bar{Q}_{44} & \bar{Q}_{45} & 0 \\ 0 & 0 & 0 & \bar{Q}_{54} & \bar{Q}_{55} & 0 \\ \bar{Q}_{61} & \bar{Q}_{62} & \bar{Q}_{63} & 0 & 0 & \bar{Q}_{66} \end{bmatrix}^k \begin{Bmatrix} \varepsilon_x \\ \varepsilon_y \\ \varepsilon_z \\ \gamma_{xz} \\ \gamma_{yz} \\ \gamma_{xy} \end{Bmatrix}^k \tag{2}$$

where $\bar{Q}_{ij}^k$ is the material constants of the *k*th ply. The transverse shear strain components in terms of the displacement components are given by

$$\begin{aligned} \gamma_{xz}^k &= \frac{\partial w_0}{\partial x} + z\frac{\partial w_1}{\partial x} + u_1 + 2zu_2 + 3z^2u_3 + \sum_{i=1}^{k-1} S_x^i H\left(z - z_i\right) \\ \gamma_{yz}^k &= \frac{\partial w_0}{\partial y} + z\frac{\partial w_1}{\partial y} + v_1 + 2zv_2 + 3z^2v_3 + \sum_{i=1}^{k-1} S_y^i H\left(z - z_i\right) \end{aligned} \tag{3}$$

Following the transverse shear free conditions at the upper and the lower surfaces of the plates, we have

$$\begin{aligned} \gamma_{xz}\big|_{z=z_1} &= \frac{\partial w_0}{\partial x} + z_1\frac{\partial w_1}{\partial x} + u_1 + 2z_1u_2 + 3z_1^2u_3 = 0 \\ \gamma_{yz}\big|_{z=z_1} &= \frac{\partial w_0}{\partial y} + z_1\frac{\partial w_1}{\partial y} + v_1 + 2z_1v_2 + 3z_1^2v_3 = 0 \end{aligned} \tag{4}$$

which are satisfied by

$$\begin{aligned} \frac{\partial w_0}{\partial x} &= H_1u_1 + H_2u_2 + H_3u_3 + H_4\frac{\partial w_1}{\partial x} \\ \frac{\partial w_0}{\partial y} &= N_1v_1 + N_2v_2 + N_3v_3 + N_4\frac{\partial w_1}{\partial y} \end{aligned} \tag{5}$$

where the expressions of H_i and N_i can be found in the Appendix.

In each interface, the continuity conditions of transverse shear stresses are

imposed, which are given by

$$\tau_{xz}^{k-1}\big|_{z=z_k} = \tau_{xz}^{k}\big|_{z=z_k}$$
$$\tau_{yz}^{k-1}\big|_{z=z_k} = \tau_{yz}^{k}\big|_{z=z_k} \tag{6}$$

From the continuity conditions of transverse shear stresses, 2(N-1) linear algebraic equations for unknowns S_x^k and S_y^k (k=1~N-1) can be set up. From the equations, variables S_x^k and S_y^k are given by

$$S_x^k = F_1^k u_1 + F_2^k u_2 + F_3^k u_3 + F_4^k \frac{\partial w_1}{\partial x} + F_5^k v_1 + F_6^k v_2 + F_7^k v_3 + F_8^k \frac{\partial w_1}{\partial y}$$
$$S_y^k = L_1^k u_1 + L_2^k u_2 + L_3^k u_3 + L_4^k \frac{\partial w_1}{\partial x} + L_5^k v_1 + L_6^k v_2 + L_7^k v_3 + L_8^k \frac{\partial w_1}{\partial y} \tag{7}$$

where the expressions of F_i^k and L_i^k can be found in the Appendix.

By using the free conditions of transverse shear stresses on the upper surface, the first derivatives of unknown variables w_1 can be eliminated from the displacement field. The final displacement fields for angle-ply laminated composite plates are now written as

$$u^k = u_0 + \Phi_1^k u_1 + \Phi^k u_2 + {}_2\Phi^k u_3 + \Phi_3^k v + {}_4\Phi_1^k v + \Phi_5^k \gamma_2$$
$$v^k = v_0 + \Psi_1^k u_1 + \Psi^k u_2 + {}_2\Psi^k u_3 + \Psi_3^k v + {}_4\Psi_1^k v + \Psi_5^k \gamma_2 \tag{8}$$
$$w = w_0 + z w_1$$

where the expressions for Φ_i^k and Ψ_i^k are given in the Appendix.

3. Finite element formulation

In equation (8), it is observed that the first derivatives of transverse displacements have been suppressed from the displacement fields of the proposed zig-zag model. Thus, C^0 interpolation functions are only required in the finite element implementation.

For the present study, a six-node triangular element with ten unknowns per node u_0, u_1, u_2, u_3, v_0, v_1, v_2, v_3, w_0, and w_1 is developed for the finite element analysis. In terms of the nodal variables and the shape functions, the displacement over an

element can be expressed as follows

$$u_0 = \sum_{i=1}^{6} N_i u_{0i}, \quad u_j = \sum_{i=1}^{6} N_i u_{ji},$$

$$v_0 = \sum_{i=1}^{6} N_i v_{0i}, \quad v_j = \sum_{i=1}^{6} N_i v_{ji}, \tag{9}$$

$$w_0 = \sum_{i=1}^{6} N_i w_{0i}, \quad w_1 = \sum_{i=1}^{6} N_i w_{1i}$$

where $N_m = (2L_m - 1)L_m$, $N_4 = 4L_1L_2$, $N_5 = 4L_2L_3$, $N_6 = 4L_3L_1$; L_m is area coordinate, $m = 1 \sim 3$; $j = 1 \sim 3$.

For linear elasticity, the strain can be written as follows

$$\begin{Bmatrix} \varepsilon_x \\ \varepsilon_y \\ \varepsilon_z \\ \gamma_{xz} \\ \gamma_{yz} \\ \gamma_{xy} \end{Bmatrix} = \begin{bmatrix} \frac{\partial}{\partial x} & 0 & 0 \\ 0 & \frac{\partial}{\partial y} & 0 \\ 0 & 0 & \frac{\partial}{\partial z} \\ \frac{\partial}{\partial z} & 0 & \frac{\partial}{\partial x} \\ 0 & \frac{\partial}{\partial z} & \frac{\partial}{\partial y} \\ \frac{\partial}{\partial y} & \frac{\partial}{\partial x} & 0 \end{bmatrix} \begin{Bmatrix} u \\ v \\ w \end{Bmatrix} = \mathbf{B}\delta^e \tag{10}$$

where $\mathbf{B} = \begin{bmatrix} B_1 & B_2 & B_3 & B_4 & B_5 & B_6 \end{bmatrix}$, $\delta^e = \begin{bmatrix} \delta_1^e & \delta_2^e & \delta_3^e & \delta_4^e & \delta_5^e & \delta_6^e \end{bmatrix}^T$, $\delta_i^e = \begin{bmatrix} u_{0i} & v_{0i} & w_{0i} & w_{1i} & u_{1i} & u_{2i} & u_{3i} & v_{1i} & v_{2i} & v_{3i} \end{bmatrix}$, $(i = 1 \sim 6)$.

$$B_i = \begin{bmatrix} \frac{\partial L_i}{\partial x} & 0 & 0 & 0 & 0 & \frac{\partial L_i}{\partial y} \\ 0 & \frac{\partial L_i}{\partial x} & 0 & 0 & 0 & \frac{\partial L_i}{\partial x} \\ 0 & 0 & 0 & \frac{\partial L_i}{\partial x} & \frac{\partial L_i}{\partial y} & 0 \\ 0 & 0 & L_i & z\frac{\partial L_i}{\partial x} & z\frac{\partial L_i}{\partial y} & 0 \\ \Phi_1^k \frac{\partial L_i}{\partial x} & \Psi_1^k \frac{\partial L_i}{\partial y} & 0 & \frac{\partial \Phi_1^k}{\partial z} L_i & \frac{\partial \Psi_1^k}{\partial z} L_i & \Phi_1^k \frac{\partial L_i}{\partial y} + \Psi_1^k \frac{\partial L_i}{\partial x} \\ \Phi_2^k \frac{\partial L_i}{\partial x} & \Psi_2^k \frac{\partial L_i}{\partial y} & 0 & \frac{\partial \Phi_2^k}{\partial z} L_i & \frac{\partial \Psi_2^k}{\partial z} L_i & \Phi_2^k \frac{\partial L_i}{\partial y} + \Psi_2^k \frac{\partial L_i}{\partial x} \\ \Phi_3^k \frac{\partial L_i}{\partial x} & \Psi_3^k \frac{\partial L_i}{\partial y} & 0 & \frac{\partial \Phi_3^k}{\partial z} L_i & \frac{\partial \Psi_3^k}{\partial z} L_i & \Phi_3^k \frac{\partial L_i}{\partial y} + \Psi_3^k \frac{\partial L_i}{\partial x} \\ \Phi_4^k \frac{\partial L_i}{\partial x} & \Psi_4^k \frac{\partial L_i}{\partial y} & 0 & \frac{\partial \Phi_4^k}{\partial z} L_i & \frac{\partial \Psi_4^k}{\partial z} L_i & \Phi_4^k \frac{\partial L_i}{\partial y} + \Psi_4^k \frac{\partial L_i}{\partial x} \\ \Phi_5^k \frac{\partial L_i}{\partial x} & \Psi_5^k \frac{\partial L_i}{\partial y} & 0 & \frac{\partial \Phi_5^k}{\partial z} L_i & \frac{\partial \Psi_5^k}{\partial z} L_i & \Phi_5^k \frac{\partial L_i}{\partial y} + \Psi_5^k \frac{\partial L_i}{\partial x} \\ \Phi_6^k \frac{\partial L_i}{\partial x} & \Psi_6^k \frac{\partial L_i}{\partial y} & 0 & \frac{\partial \Phi_6^k}{\partial z} L_i & \frac{\partial \Psi_6^k}{\partial z} L_i & \Phi_6^k \frac{\partial L_i}{\partial y} + \Psi_6^k \frac{\partial L_i}{\partial x} \end{bmatrix}^T \tag{11}$$

The element stiffness matrix can be expressed as

$$\mathbf{K}^e = \int_e \mathbf{B}^T \mathbf{Q} \mathbf{B} dv \tag{12}$$

where $\mathbf{Q}$ is the transformed material constant matrix.

By employing the virtual work principle and equating work done to internal forces, the following system equation can be derived.

$$\mathbf{K}\boldsymbol{\delta} = \mathbf{P} \tag{13}$$

where $\mathbf{K} = \sum_{e=1}^{NE} \mathbf{K}^e$, $\mathbf{P} = \sum_{e=1}^{NE} \mathbf{P}^e$; $\mathbf{P}^e$ is nodal load vector for one element; *NE* is the total number of elements.

4. Numerical results and discussions

In this section, several examples of bending of angle-ply composite plates subjected to various boundary conditions are studied to assess the performance of the proposed C^0 zig-zag model. As for C^1-type zig-zag model [18], only analytical

solution for cross-ply plates is available in the literature, however in this paper finite element results of the angle-ply composite plates using the refined nonconforming element method proposed by Cheung and Chen [32] will be presented. Chakrabarti and Sheikh [33] attempted to developed a six-node triangular element based on the zig-zag theory for the free vibration analysis of sandwich plates. The six-node plate element developed is a nonconforming element as the element does not satisfy the normal slope continuity requirement. Thus, Kulkarni and Kapuria [34] indicated that the six-node triangular element [33] underestimated the natural frequencies of the sandwich plates. Therefore, three-node triangular element based on the C^1-type zig-zag model [18] has been developed for comparison in this paper.

4.1 Material constants

Material (1) for laminated composite plates [35]

$$E_1 = 172.5GPa,\ \ E_2 = E_3 = 6.9GPa,\ \ G_{12} = G_{13} = 3.45GPa,$$

$$G_{23} = 1.38GPa,\ \ v_{12} = v_{13} = v_{23} = 0.25.$$

Material (2) for laminated composite plates [36]

$$C_{11} = 1.0025E_2,\ \ C_{12} = 0.25E_2,\ \ C_{22} = 25.0625E_2,\ \ C_{33} = C_{11},$$

$$C_{44} = 0.5E_2,\ \ C_{55} = 0.2E_2,\ \ C_{66} = C_{44}.$$

Material (3) for laminated composite plates [36]

$$C_{11} = 32.0625E_2,\ \ C_{12} = 0.2495E_2,\ \ C_{22} = 1.00195E_2,\ \ C_{33} = C_{22},$$

$$C_{44} = 0.2E_2,\ \ C_{55} = 0.8E_2,\ \ C_{66} = C_{55}.$$

Material (4) for laminated composite plates [36]

$$C_{11} = 25.0625E_2,\ \ C_{12} = 0.25E_2,\ \ C_{22} = 1.0025E_2,\ \ C_{33} = C_{22},$$

$$C_{44} = 0.2E_2,\ \ C_{55} = 0.5E_2,\ \ C_{66} = C_{55}.$$

where 1 and 2 denote the in-plane directions; 3 denotes transverse direction of laminates.

4.2 Boundary conditions

Several types of boundary conditions are used in the examples, such as simply-supported boundary conditions and clamped boundary conditions, which are presented as follows.

Simply supported boundary conditions on all sides of the composite plates (SSSS):

$v_0=w_0= w_1=v_1=v_2=v_3=0$ at $x=0, a$;

$u_0=w_0= w_1=u_1=u_2=u_3=0$ at $y=0, b$.

Simply-free conditions at two opposite edges has been considered. This plate is simply supported along the edges parallel to the y-axis while the other two edges are free (SFSF):

$w_0= w_1 =0$ at $x=0, a$.

Clamp-free conditions at two opposite edges has been considered. This plate is clamped along the edges parallel to the y-axis while the other two edges are free (CFCF):

$u_0=v_0=w_0= w_1=u_1=u_2=u_3=v_1=v_2=v_3=0$ at $x=0, a$.

In the tables and the figures, the following non-dimensional displacement and stresses are evaluated:

$$\bar{u}=\frac{E_2 u h^2}{q_0 a^3},\quad \bar{w}=100E_2h^3w(0,0,z)/q_0L^4,\quad \bar{\sigma}_x=\frac{\sigma_x h^2}{q_0 a^2},\quad \bar{\tau}_{xy}=\frac{\tau_{xy}h^2}{q_0a^2},\quad \bar{\tau}_{xz}=\frac{\tau_{xz}h}{q_0a},$$

$$\tilde{u}=\frac{E_2 u}{q_0 h},\quad \tilde{\sigma}_x=\frac{\sigma_x}{q_0},\quad \tilde{\tau}_{xy}=\frac{\tau_{xy}(a/2,b/2,z)}{q_0},\quad \tilde{\tau}_{xz}=\frac{\tau_{xz}}{q_0},\quad \tilde{\tau}_{yz}=\frac{\tau_{yz}}{q_0}.$$

Example 1: Laminated composite plates subjected to double sinusoidal normal pressure $q=q_0\sin\pi x/a\sin\pi y/b$ on the top surface ($z=h/2$). In this example, the cross-ply laminated composite plates ($b/a=1$) having antisymmetric and symmetric lamination schemes $[0^\circ/90^\circ]$ and $[0^\circ/90^\circ/0^\circ]$ are considered for simply-supported boundary condition on all sides (SSSS).

The finite element meshes for the static analysis of the composite plates are shown in Figure 2. In order to determine the required mesh density $N\times N$ for results of acceptable accuracy, a convergence study has been carried out. Figure 3 shows the convergence of transverse displacement for two-ply plate $[0^\circ/90^\circ]$ with material (1) where the mesh size parameter N is varied from 2 to 16. Acronym ZZTC-C0 represents the results obtained from the six-node triangular element based on the

proposed C^0-type zig-zag model with 10 unknowns at each node. HSDT-98 denotes the results obtained from the six-node triangular element based on the nine-order theory [37] with 29 unknowns at each node. ZZTC-C1 represents the results obtained from the three-node triangular element based on the C^1-type zig-zag theory [18] in which the refined nonconforming element method proposed by Cheung and Chen [32] is used to circumvent the requirement of C^1 continuity, and 13 variables are defined at each node. It can be found that the values of transverse displacement converge for N=12, so that all subsequent analysis are carried out with a mesh size of 12×12 for six-node triangular element. However, a mesh size of 24×24 will be used for the three-node triangular element (ZZTC-C1), so that the number of nodes are the same for the two meshes.

For moderately thick two-ply plate (a/h=4), comparison of in-plane displacement computed from different models is shown in Figure 4. It is observed that the results ZZTC-C0 and HSDT-98 are in close agreement with the three-dimensional elasticity solutions (Exact). Distributions of in-plane stresses through the thickness are shown in Figures 5 and 6. It is found that the model ZZTC-C0 can produce much better in-plane stress distributions through the thickness. However, the results ZZTC-C1 obtained from C^1-type zig-zag theory [18] are less accurate. The distributions of transverse shear stresses along the thickness are shown in Figure 7. It is found that transverse shear stress ZZTC-C1-E obtained by integrating three-dimensional equilibrium equations within one element is even worse than the ZZTC-C1-C obtained directly from the constitutive equations. For three-node triangular element, the interpolation functions of in-plane displacement parameters are linear which cannot provide contribution to transverse shear stresses based on the three-dimensional equilibrium consideration. As a result, for C^1-type zig-zag model, transverse shear stresses are computed directly from the constitutive equations. However, for other models, transverse shear stresses are obtained by integrating three-dimensional equilibrium equations.

For a two-ply thick plate (a/h=2), comparisons of in-plane displacement and stress components are shown in Figures 8 and 9. It is found that results obtained from the model ZZTC-C0 are in good agreement with the three-dimensional elasticity solutions [37]. However, results obtained from the model ZZTC-C1 are less promising. For the model ZZTC-C1, the maximum percentage errors relative to the three dimensional elasticity solutions are more than 50%. Moreover, the results obtained from the first-order shear deformation theory (FSDT) are also disappointing.

Involving 29 variables in the displacement field, the model HSDT-98 could produce reliable accurate results, so HSDT-98 is chosen as reference for possible comparisons.

For a three-ply thin plate [0°/90°/0°], transverse displacement and in-plane stresses computed from the proposed six-node triangular element are compared to three-dimensional elasticity solutions (Exact) and the results obtained from the classical laminated plate theory (CLPT) in Table 1. Numerical results show that the present six-node triangular element is free from the shear locking problem.

Example 2: Laminated composite plates subjected to sinusoidal normal pressure $q=q_0\sin\pi x/a$ on the top surface ($z=h/2$). In this example, the laminated composite plates ($b/a=1$) with material (1) having antisymmetric lamination scheme [15°/-15°] and arbitrary lamination scheme [15°/30°/0°/-45°/-15°] are studied for the simply-free conditions (SFSF) and the clamp-free conditions at two opposite edges (CFCF).

In Tables 2 and 3, the values of in-plane and transverse shear stresses are presented for two-ply plate [15°/-15°] ($a/h=4$), respectively. It is found in the Tables that the present results ZZTC-C0 agree well with the exact solutions given by Ren [38] using Pagano's approach [39] and the three-dimensional results [40]. For two-ply moderately thick plate [15°/-15°] ($a/h=4$), comparisons of displacements and stresses are clearly shown in Figures 10-13. Subsequently, results of thick plate ($a/h=2.5$) are shown in Figures 14-17. It can be found that with an increase in the thickness of the plate, accuracy of the model ZZTC-C1 [18] further deteriorates.

For the five-layer [−15°/−45°/0°/30°/15°] plate ($a/h=4$) with the simply-free conditions (SFSF), the results are respectively presented to compared with three-dimensional elasticity solution (3-D) [41] in Figures 18-20. Subsequently, the results of five-layer plates ($a/h=4$) with the clamp-free conditions (CFCF) are respectively plotted in Figures 21-23. It is noted in Figures 18-23 that for five-layer angle-ply plate with the same length-to-thickness ratio ($a/h=4$), the accuracy of the model ZZTC-C1 [18] decreases rapidly for the clamp-free conditions (CFCF). Figures 24-26 present the distributions of displacements and stresses for the five-layer thick plate ($a/h=2.5$) with the simply-free conditions (SFSF). As for the distributions of displacements and stresses for the five-layer thick plate ($a/h=2.5$) with the clamp-free

conditions (CFCF), they are plotted in Figures 27-29.

Example 3: Simply-supported laminated composite plate (SSSS) with different thickness and material properties at each ply. The laminated composite plate subjected to a doubly sinusoidal transverse loading $q = q_0 \sin(\pi x/a)\sin(\pi y/b)$. The plies of the composite plate are of thickness $0.3h/0.2h/0.15h/0.25h/0.1h$ and of materials 4/2/4/3/2.

To further assess the performance of the proposed model, a five-layer plate with different thickness and material properties at each ply is studied in this example. Distributions of displacement and stresses through the thickness are shown in Figures 30-33. With the rapid changes of material properties through the thickness direction for the five-layer plate, results (ZZT) obtained from the postprocessing method proposed by Cho and Choi [36] are less accurate. Again, it is observed that the results obtained from the proposed model ZZTC-C0 are in close agreement with the reference results of HSDT-98.

5. Conclusions

In this paper, a C^0-type zig-zag plate model (ZZTC-C0) is presented for the analysis of laminated composite plates with general angle-ply configurations. The proposed model satisfies the transverse shear free conditions at the top and bottom surfaces and interlaminar shear stress continuity at interfaces. Derivatives of transverse displacements have been eliminated from the displacement field, so that a C^0 finite element can be formulated. With mesh refinement, convergence can be achieved, which shows that the accurate results can be obtained by using relatively fewer elements. Many problems have been analyzed covering different features of laminated composite plates such as ply orientations, boundary conditions and length-to-thickness ratio. Numerical results show that the proposed zig-zag model is capable to produce results close to the three dimensional elasticity solutions for laminated composite plates with general lamination configurations. The available C^1-type zig-zag model (ZZTC-C1) is less promising for laminated composite under simply-supported boundary conditions. Moreover, the accuracy of the model ZZTC-C1 deteriorates rapidly for the clamped boundary conditions, in particular with an increase of plate thickness. There are 13 variables at each node in the displacement field of ZZTC-C1, whereas only 10 variables are involved in the displacement field of the proposed model ZZTC-C0. Nevertheless, the newly developed model ZZTC-C0

making use of all stress compatibility conditions can produce results with accuracy comparable to the much more costly model HSDT-98.

Acknowledgement

The work described in this paper was supported by the HKSAR GRR Grant to the research project HKU715110E on “Drift based seismic fragility analysis of high-rise RC building with transfer structures”, the National Natural Sciences Foundation of China [No. 11272217, 11402152].

Appendix

$$\Phi_1^k = \sum_{i=1}^{k} \left(F_1^k + F_4^k A_1 + F_8^k B_1 \right) \left(z_{\bar{i}} \right) z \text{ -},$$

$$\Phi_2^k = \sum_{i=1}^{k} \left(F_2^k + F_4^k A_2 + F_8^k B_2 \right) \left(z_{\bar{i}} \right) z^2 +,$$

$$\Phi_3^k = \sum_{i=1}^{k} \left(F_3^k + F_4^k A_3 + F_8^k B_3 \right) \left(z_{\bar{i}} \right) z^3 +,$$

$$\Phi_4^k = \sum_{i=1}^{k} \left(F_5^k + F_4^k A_4 + F_8^k B_4 \right) \left(z_{\bar{i}} \right),$$

$$\Phi_5^k = \sum_{i=1}^{k} \left(F_6^k + F_4^k A_5 + F_8^k B_5 \right) \left(z_{\bar{i}} \right),$$

$$\Phi_6^k = \sum_{i=1}^{k} \left(F_7^k + F_4^k A_6 + F_8^k B_6 \right) \left(z_{\bar{i}} \right);$$

$$\Psi_1^k = \sum_{i=1}^{k} \left(L_1^k + L_4^k A_1 + L_8^k B_1 \right) \left(z_{\bar{i}} \right),$$

$$\Psi_2^k = \sum_{i=1}^{k} \left(L_2^k + L_4^k A_2 + L_8^k B_2 \right) \left(z_{\bar{i}} \right),$$

$$\Psi_3^k = \sum_{i=1}^{k} \left(L_3^k + L_4^k A_3 + L_8^k B_3 \right) \left(z_{\bar{i}} \right),$$

$$\Psi_4^k = \sum_{i=1}^{k} \left(L_5^k + L_4^k A_4 + L_8^k B_4 \right) z^{-i},$$

$$\Psi_5^k = \sum_{i=1}^{k} \left(L_6^k + L_4^k A_5 + L_8^k B_5 \right) z^{-i},$$

$$\Psi_6^k = \sum_{i=1}^{k} \left(L_7^k + L_4^k A_6 + L_8^k B_6 \right) z^{-i}.$$

where

$$A_1 = -\left(\beta_8\alpha_1 - \alpha_8\beta_1\right)/\left(\beta_8\alpha_4 - \alpha_8\beta_4\right), \quad A_2 = -\left(\beta_8\alpha_2 - \alpha_8\beta_2\right)/\left(\beta_8\alpha_4 - \alpha_8\beta_4\right),$$

$$A_3 = -\left(\beta_8\alpha_3 - \alpha_8\beta_3\right)/\left(\beta_8\alpha_4 - \alpha_8\beta_4\right), \quad A_4 = -\left(\beta_8\alpha_5 - \alpha_8\beta_5\right)/\left(\beta_8\alpha_4 - \alpha_8\beta_4\right),$$

$$A_5 = -\left(\beta_8\alpha_6 - \alpha_8\beta_6\right)/\left(\beta_8\alpha_4 - \alpha_8\beta_4\right), \quad A_6 = -\left(\beta_8\alpha_7 - \alpha_8\beta_7\right)/\left(\beta_8\alpha_4 - \alpha_8\beta_4\right);$$

$$B_1 = -\left(\alpha_4\beta_1 - \beta_4\alpha_1\right)/\left(\beta_8\alpha_4 - \alpha_8\beta_4\right), \quad B_2 = -\left(\alpha_4\beta_2 - \beta_4\alpha_2\right)/\left(\beta_8\alpha_4 - \alpha_8\beta_4\right),$$

$$B_3 = -\left(\alpha_4\beta_3 - \beta_4\alpha_3\right)/\left(\beta_8\alpha_4 - \alpha_8\beta_4\right), \quad B_4 = -\left(\alpha_4\beta_5 - \beta_4\alpha_5\right)/\left(\beta_8\alpha_4 - \alpha_8\beta_4\right),$$

$$B_5 = -\left(\alpha_4\beta_6 - \beta_4\alpha_6\right)/\left(\beta_8\alpha_4 - \alpha_8\beta_4\right), \quad B_6 = -\left(\alpha_4\beta_7 - \beta_4\alpha_7\right)/\left(\beta_8\alpha_4 - \alpha_8\beta_4\right).$$

where

$$\alpha_1 = \sum_{i=1}^{N-1} F_1^i + H_1 + 1, \quad \alpha_2 = \sum_{i=1}^{N-1} F_2^i + H_2 + 2z, \quad \alpha_3 = \sum_{i=1}^{N-1} F_3^i + H_3 + 3z^2,$$

$$\alpha_4 = \sum_{i=1}^{N-1} F_4^i + H_4 + i, \quad \alpha_5 = \sum_{i=1}^{N-1} F_5^i, \quad \alpha_6 = \sum_{i=1}^{N-1} F_6^i, \quad \alpha_7 = \sum_{i=1}^{N-1} F_7^i, \quad \alpha_8 = \sum_{i=1}^{N-1} F_8^i;$$

$$\beta_1 = \sum_{i=1}^{N-1} L_1^i, \quad \beta_2 = \sum_{i=1}^{N-1} L_2^i, \quad \beta_3 = \sum_{i=1}^{N-1} L_3^i, \quad \beta_4 = \sum_{i=1}^{N-1} L_4^i, \quad \beta_5 = \sum_{i=1}^{N-1} L_5^i + N_1 + 1,$$

$$\beta_6 = \sum_{i=1}^{N-1} L_6^i + N_2 - 2i, \quad \beta_7 = \sum_{i=1}^{N-1} L_7^i + N_3 + 3z^2, \quad \beta_8 = \sum_{i=1}^{N-1} L_8^i + N_4 + z.$$

For k =1, the coefficients F_i^k and L_i^k are given by

$$F_1^1=\mu_1^1\left(1+H_1\right),\ \ F_2^1=\mu_1^1\left(2z+H_2\right),\ \ F_3^1=\mu_1^1\left(3z^2+H_3\right),\ \ F_4^1=\mu_1^1\left(z+H_4\right),$$

$$F_5^1=\mu_2^1\left(1+N_1\right),\ \ F_6^1=\mu_2^1\left(2z+N_2\right),\ \ F_7^1=\mu_2^1\left(3z^2+N_3\right),\ \ F_8^1=\mu_2^1\left(z+N_4\right).$$

$$L_1^1=\nu_1^1\left(1+H_1\right),\ \ L_2^1=\nu_1^1\left(2z+H_2\right),\ \ L_3^1=\nu_1^1\left(3z^2+H_3\right),\ \ L_4^1=\nu_1^1\left(z+H_4\right),$$

$$L_5^1=\nu_2^1\left(1+N_1\right),\ \ L_6^1=\nu_2^1\left(2z+N_2\right),\ \ L_7^1=\nu_2^1\left(3z^2+N_3\right),\ \ L_8^1=\nu_2^1\left(z+N_4\right).$$

For k > 1, the coefficients F_i^k can be obtained from the following recursive equations.

$$F_1^k=\mu_1^k\sum_{i=1}^{k-1}F_1^i+\mu_2^k\sum_{i=1}^{k-1}L_1^i+\mu_1^k\left(1+H_1\right),\ \ F_2^k=\mu_1^k\sum_{i=1}^{k-1}F_2^i+\mu_2^k\sum_{i=1}^{k-1}L_2^i+\mu_1^k\left(2z+H_2\right),$$

$$F_3^k=\mu_1^k\sum_{i=1}^{k-1}F_3^i+\mu_2^k\sum_{i=1}^{k-1}L_3^i+\mu_1^k\left(3z^2+H_3\right),\ \ F_4^k=\mu_1^k\sum_{i=1}^{k-1}F_4^i+\mu_2^k\sum_{i=1}^{k-1}L_4^i+\mu_1^k\left(z+H_4\right),$$

$$F_5^k=\mu_1^k\sum_{i=1}^{k-1}F_5^i+\mu_2^k\sum_{i=1}^{k-1}L_5^i+\mu_2^k\left(1+N_1\right),\ \ F_6^k=\mu_1^k\sum_{i=1}^{k-1}F_6^i+\mu_2^k\sum_{i=1}^{k-1}L_6^i+\mu_2^k\left(2z+N_2\right),$$

$$F_7^k=\mu_1^k\sum_{i=1}^{k-1}F_7^i+\mu_2^k\sum_{i=1}^{k-1}L_7^i+\mu_2^k\left(3z^2+N_3\right),\ \ F_8^k=\mu_1^k\sum_{i=1}^{k-1}F_8^i+\mu_2^k\sum_{i=1}^{k-1}L_8^i+\mu_2^k\left(z+N_4\right);$$

$$L_1^k=\nu_1^k\sum_{i=1}^{k-1}F_1^i+\nu_2^k\sum_{i=1}^{k-1}L_1^i+\nu_1^k\left(1+H_1\right),\ \ L_2^k=\nu_1^k\sum_{i=1}^{k-1}F_2^i+\nu_2^k\sum_{i=1}^{k-1}L_2^i+\nu_1^k\left(2z+H_2\right),$$

$$L_3^k=\nu_1^k\sum_{i=1}^{k-1}F_3^i+\nu_2^k\sum_{i=1}^{k-1}L_3^i+\nu_1^k\left(3z^2+H_3\right),\ \ L_4^k=\nu_1^k\sum_{i=1}^{k-1}F_4^i+\nu_2^k\sum_{i=1}^{k-1}L_4^i+\nu_1^k\left(z+H_4\right),$$

$$L_5^k=\nu_1^k\sum_{i=1}^{k-1}F_5^i+\nu_2^k\sum_{i=1}^{k-1}L_5^i+\nu_2^k\left(1+N_1\right),\ \ L_6^k=\nu_1^k\sum_{i=1}^{k-1}F_6^i+\nu_2^k\sum_{i=1}^{k-1}L_6^i+\nu_2^k\left(2z+N_2\right),$$

$$L_7^k=\nu_1^k\sum_{i=1}^{k-1}F_7^i+\nu_2^k\sum_{i=1}^{k-1}L_7^i+\nu_2^k\left(3z^2+N_3\right),\ \ L_8^k=\nu_1^k\sum_{i=1}^{k-1}F_8^i+\nu_2^k\sum_{i=1}^{k-1}L_8^i+\nu_2^k\left(z+N_4\right).$$

where

$$H_1 = -1,\ \ H_2 = -2z_1,\ \ H_3 = -3z_1^2,\ \ H_4 = -z_1\ ;$$

$$N_1 = -1,\ \ N_2 = -2z_1,\ \ N_3 = -3z_1^2,\ \ N_4 = -z_1\ ;$$

$$\mu_1^k = \frac{Q_{55}^{k+1}\left(Q_{44}^{k}\overline{\ }\ Q_{44}^{k+1}\right) - Q^{k+1}\left(_{45}Q^{k}\right.\overline{\ }\ _{54}Q\left.\right)^{k+1}}{Q_{44}^{k+1}Q_{55}^{k+1}\overline{\ } - Q_{45}^{k+1}Q_{54}^{k+1}},$$

$$\mu_2^k = \frac{Q_{55}^{k+1}\left(Q_{45}^{k}\overline{\ }\ Q_{45}^{k+1}\right) - Q^{k+1}\left(_{45}Q^{k}\right.\overline{\ }\ _{55}Q\left.\right)^{k+1}}{Q_{44}^{k+1}Q_{55}^{k+1}\overline{\ } - Q_{45}^{k+1}Q_{54}^{k+1}},$$

$$\nu_1^k = \frac{Q_{44}^{k+1}\left(Q_{54}^{k}\overline{\ }\ Q_{54}^{k+1}\right) - Q^{k+1}\left(_{54}Q^{k}\right.\overline{\ }\ _{44}Q\left.\right)^{k+1}}{Q_{44}^{k+1}Q_{55}^{k+1}\overline{\ } - Q_{45}^{k+1}Q_{54}^{k+1}},$$

$$\nu_2^k = \frac{Q_{44}^{k+1}\left(Q_{55}^{k}\overline{\ }\ Q_{55}^{k+1}\right) - Q^{k+1}\left(_{54}Q^{k}\right.\overline{\ }\ _{45}Q\left.\right)^{k+1}}{Q_{44}^{k+1}Q_{55}^{k+1}\overline{\ } - Q_{45}^{k+1}Q_{54}^{k+1}}.$$

References

[1] Carrera E, C_z^0 requirements-models for the two dimensional analysis of multilayered structures. Compos Struct, 1997; 37:373-383.

[2] Murakami H, Laminated composite plate theory with improved in-plane response. J Appl Mech, 1986; 53:661-666.

[3] Murakami H, Toledano A, A higher-order laminated plate theory with improved in-plane response. Int J Solids Struct, 1987; 23(1):111-131.

[4] Brischetto S, Carrera E, Demasi L, Improved bending analysis of sandwich plates using a zig-zag function. Compos Struct, 2009; 89:408-415.

[5] Carrera E. On the use of the Murakami's zig-zag function in the modeling of layered plates and shells. Comput Struct, 2004; 82:541-554.

[6] Rodrigues JD, Roque CMC, Ferreira AJM, Carrera E, Cinefra M, Radial basis functions-finite differences collocation and a unified formulation for bending, vibration and buckling analysis of laminated plates, according to Murakami's zig-zag theory. Compos Struct, 2011; 93:1613-1620.

[7] Neves AMA, Ferreira AJM, Carrera E, Cinefra M. Jorge RMN, Soares CMM, Static analysis of functionally graded sandwich plates according to a hyperbolic theory considering zig-zag and warping effects. Advances in Engineering Software, 2012; 52:30-43.

[8] Rodrigues JD, Roque CMC, Ferreira AJM, Cinefra M, Carrera E, Radial basis functions-differential quadrature collocation and a unified formulation for bending, vibration and buckling analysis of laminated plates, according to Murakami's Zig-Zag theory. Comput Struct, 2012; 90-91:107-115.

[9] Dafedar JB, Desai YM, Mufti AA, Stability of sandwich plates by mixed, higher-order analytical formulation. Int J Solids Struct, 2003; 40:4501-4517.

[10] Di Sciuva M. Multilayered anisotropic plate models with continuous interlaminar stresses. Compos Struct, 1992; 22:149-167.

[11] Cho M, Parmerter RR. An efficient higher-order plate theory for laminated composites. Compos Struct, 1992; 20:113-123.

[12] Cho M, Kim JS, Four-noded finite element post-process method using a displacement field of higher-order laminated composite plate theory. Comput Struct, 1996; 61:283-290.

[13] Chakrabarti A and Sheikh AH, A new triangular element to model inter-laminar shear stress continuous plate theory. Int J Numer Methods Eng, 2004; 60:1237-1257.

[14] Kapuria S, Dumir PC, Jain NK. Assessment of zigzag theory for static loading, buckling, free and forced response of composite and sandwich beams. Compos Struct, 2004; 64:317-327.

[15] Chakrabarti A and Sheikh AH, Analysis of laminated sandwich plates based on interlaminar shear stress continuous plate theory. J Eng Mech, 2005; 131: 377-384.

[16] Ali JSM, Bhaskar K, Varadan TK, A new theory for accurate thermal/mechanical flexural analysis of symmetric laminated plates. Compos Struct, 1999; 45:227-232.

[17] Cho M, Oh J, Higher order zig-zag theory for fully coupled thermo-electric-mechanical smart composite plates. Int J Solids Struct, 2004;

41:1331-1356.

[18] Cho M, Oh J, Higher order zig-zag plate theory under thermo-electric-mechanical loads combined. Composites: Part B, 2003; 34:67-82.

[19] Oh J, Cho M, A finite element based on cubic zig-zag plate theory for the prediction of thermo-electric-mechanical behaviors. Int J Solids Struct, 2004; 41:1357-1375.

[20] Specht B, Modified shape function for the three-node plate bending element passing the patch test. Int J Numer Methods Eng, 1988; 26:705-715.

[21] Carrera E, Historical review of zig-zag theories for multilayered plates and shells. Applied Mechanics Reviews, 2003; 56:287-308.

[22] Pandit MK, Singh BN, Sheikh AH, Buckling of laminated sandwich plates with soft core based on an improved higher order zigzag theory, Thin-Walled Structures, 2008; 46:1183-1191.

[23] Pandit MK, Singh BN, Sheikh AH, Vibration of sandwich plates with random material properties using improved higher-order zig-zag theory. Mechanics of Advanced Materials and Structures, 2010; 17:561-572.

[24] Pandit MK, Singh BN, Sheikh AH, Stochastic free vibration of soft core sandwich plates using an improved higher-order zig-zag theory. 2010; 23: 14-23.

[25] Singh SK, Chakrabarti A, Buckling analysis of laminated composite plates using an efficient C^0 FE model. Latin American Journal of Solids and Structures, 2012; 1:1-13.

[26] Khandelwal RP, Chakrabarti A, Bhargava P, An efficient FE model and Least Square Error method for accurate calculation of transverse shear stresses in composites and sandwich laminates. Composites: Part B, 2012; 43:1695-1704.

[27] Kumar A, Chakrabarti A, Bhargava P, Finite element analysis of laminated composite and sandwich shells using higher-order zigzag theory. Compos Struct, 2013; 106:270-281.

[28] Ren XH, Chen WJ, Wu Z, A new zig-zag theory and C^0 plate bending element for composite and sandwich plates. Arch Appl Mech, 2011; 81:185-197.

[29] Wu Z, SH Lo, Ren XH, Effects of displacement parameters in zig-zag theories on displacements and stresses of laminated composites. Compos Struct, 2014;

110:276-288.

[30] Matsunaga H, Free vibration and stability of angle-ply laminated composite and sandwich plates under thermal loading. Compos Struct, 2007; 77:249-262.

[31] Zenkour AM, Hygrothermal effects on the bending of angle-ply composite plates using a sinusoidal theory. Compos Struct, 2012; 94:3685-3696.

[32] Y.K. Cheung, Chen WJ, Refined nine-parameter triangular thin plate bending element by using refined direct stiffness method, Int J Numer Methods Eng, 1995; 38: 283-298.

[33] Chakrabarti A, Sheikh AH, Vibration of laminate-faced sandwich plate by a new refined element. J Aerospace Eng, 2004; 17:123-134.

[34] Kulkarni SD, Kapuria S, Free vibration analysis of composite and sandwich plates using an improved discrete Kirchhoff quadrilateral element based on third-order zigzag theory. Comput Mech, 2008; 42:803-824.

[35] Pagano NJ, Exact solutions for rectangular bi-directional composites. J Compos Mater, 1970 ; 4: 20-34.

[36] Cho M, Choi YJ, A new postprocessing method for laminated composites of general lamination configurations. Compos Struct, 2001; 54:397-406.

[37] Matsunaga H, Assessment of a global higher-order deformation theory for laminated composite and sandwich plates. Compos Struct, 2002; 56:279-291.

[38] Ren JG, Bending theory of laminated plate. Compos Sci Tech, 1986; 27:225-248.

[39] Pagano NJ, Influence of shear coupling in cylindrical bending of anisotropic laminates. J Compos Mater, 1970; 4:330-343.

[40] Bogdanovich AE, Yushanov SP, Three-dimensional variational analysis of Pagano's problems for laminated composite plates. Compos Sci Tech, 2000; 60:2407-2425.

[41] Chen WQ, Lee KY, Three-dimensional exact analysis of angle-ply laminates in cylindrical bending with interfacial damage via state-space method. Compos Struct, 2004; 64:275-283.

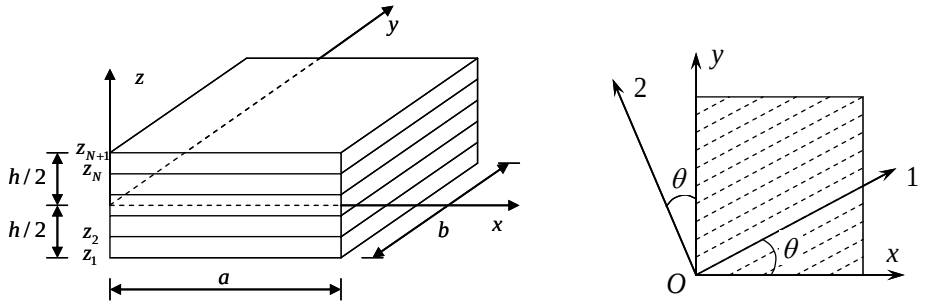

Fig. 1 Schematic diagram for the angle-ply laminated plate segment and material coordinates axes $O12$

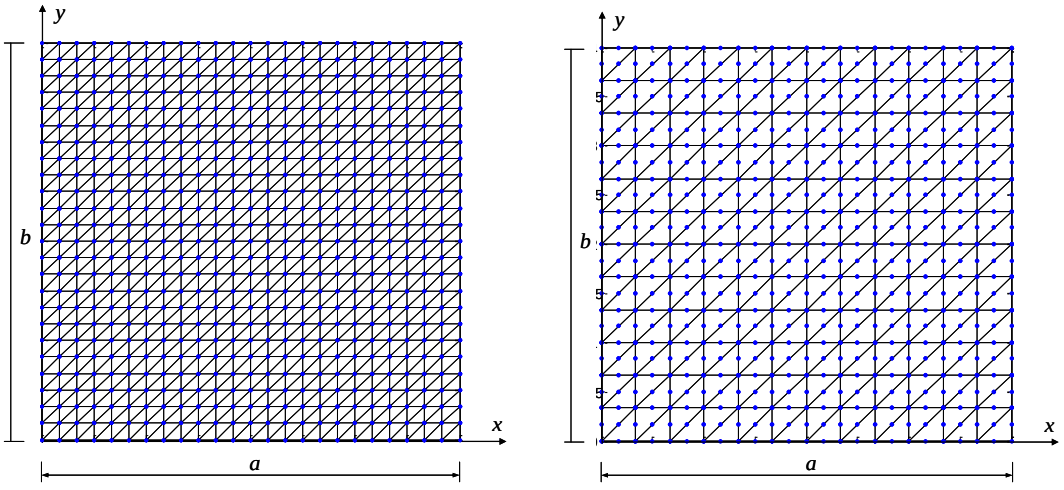

(*a*) The 24×24 finite element meshes of three-node triangular element

(*b*) The 12×12 finite element meshes of six-node triangular element

Fig. 2 The finite element meshes of the entire plate

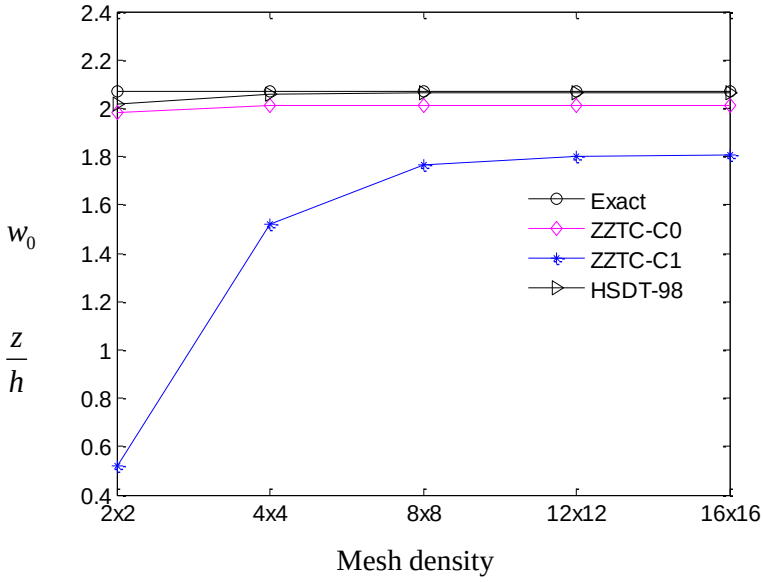

Fig. 3 Convergence rate of transverse displacement for two-ply [$0^\circ / 90^\circ$] plate (a/h=4)

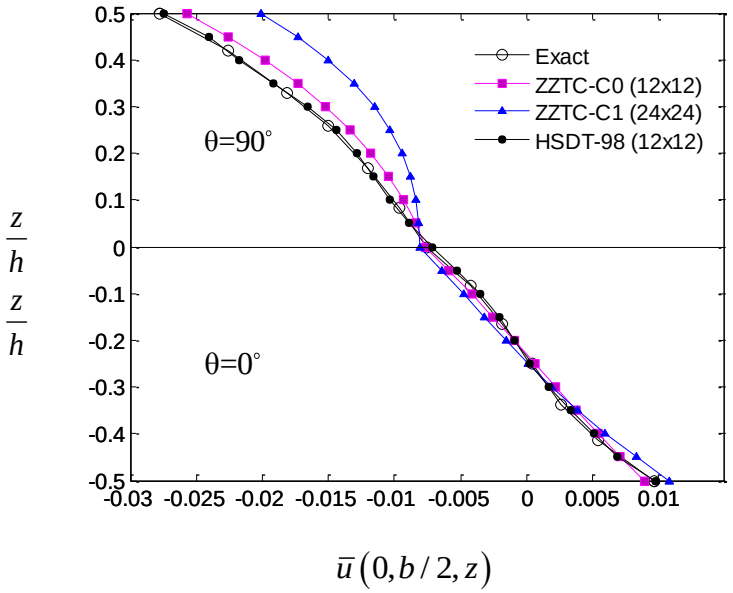

Fig. 4 Distribution of in-plane displacement through thickness of two-layer [$0^\circ / 90^\circ$] plate (a/h=4)

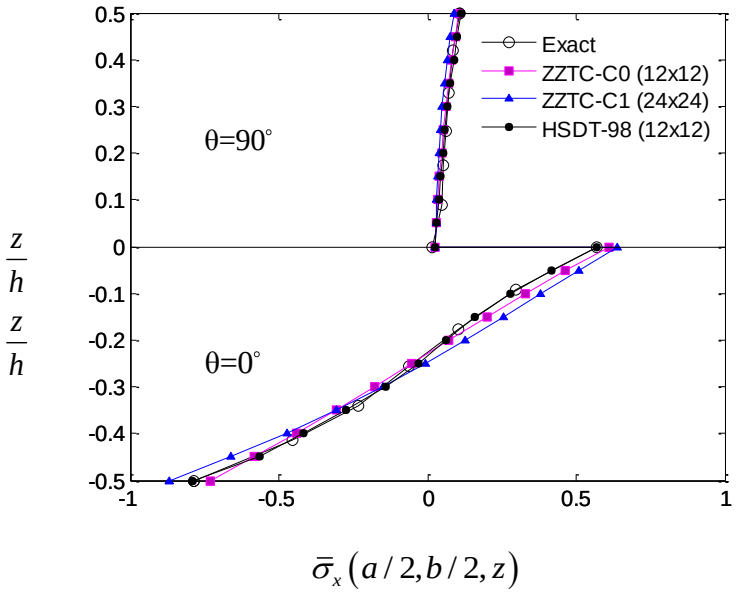

Fig. 5 Distribution of in-plane stress through thickness of two-layer [$0^\circ/90^\circ$] plate (a/h=4)

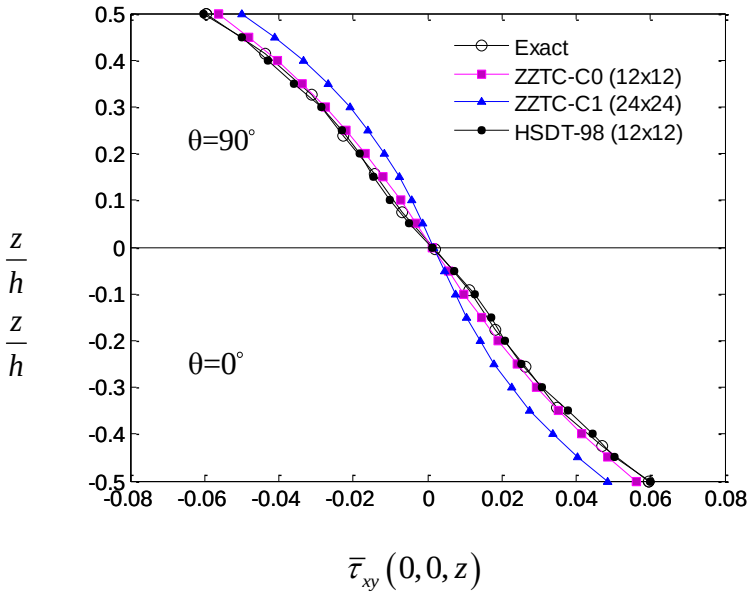

Fig. 6 Distribution of in-plane stress through thickness of two-layer [$0^\circ/90^\circ$] plate (a/h=4)

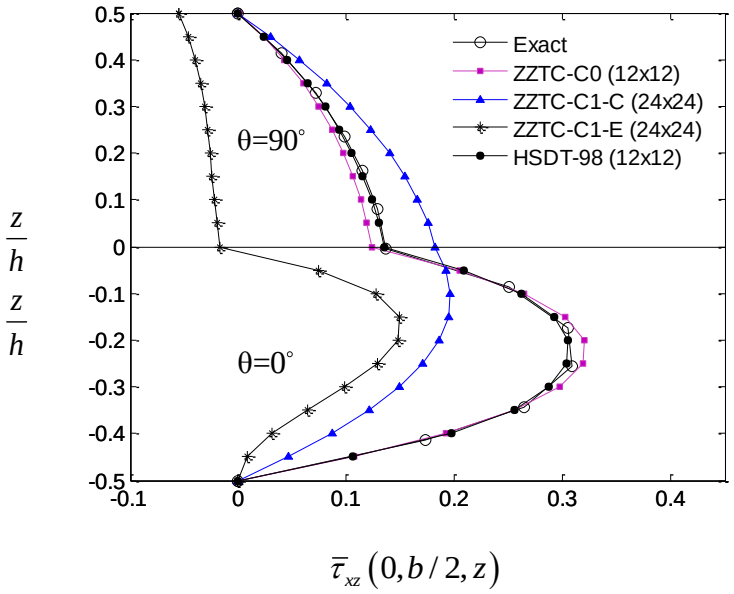

Fig. 7 Distribution of transverse shear stress through thickness of two-layer [$0^\circ / 90^\circ$] plate (a/h=4)

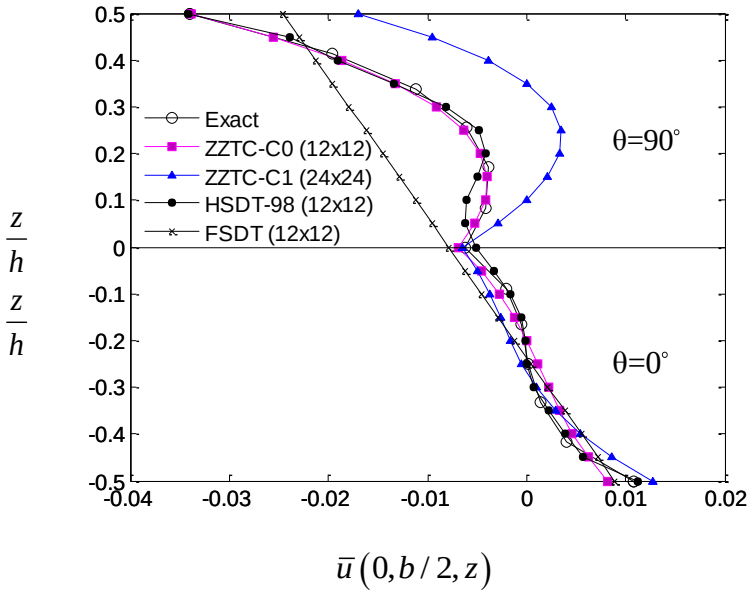

Fig. 8 Distribution of in-plane displacement through thickness of two-layer [$0^\circ / 90^\circ$] plate (a/h=2)

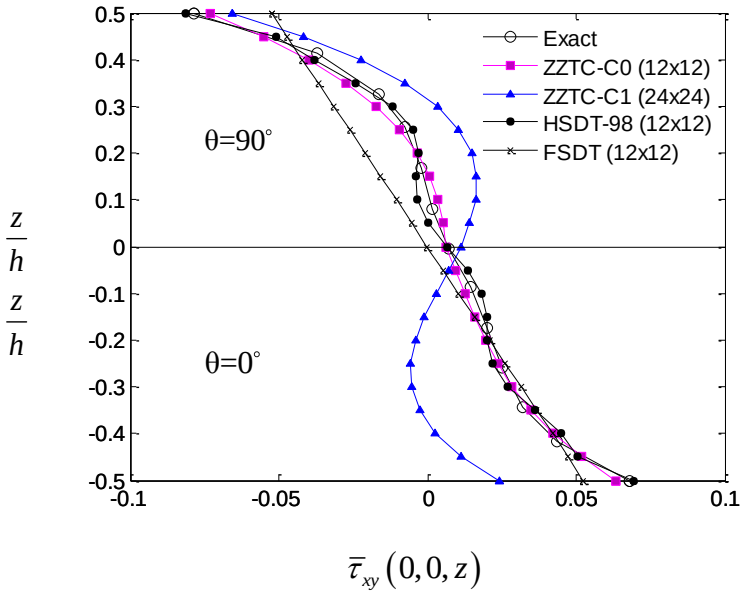

Fig. 9 Distribution of in-plane stress through thickness of two-layer [$0^\circ/90^\circ$] plate (a/h=2)

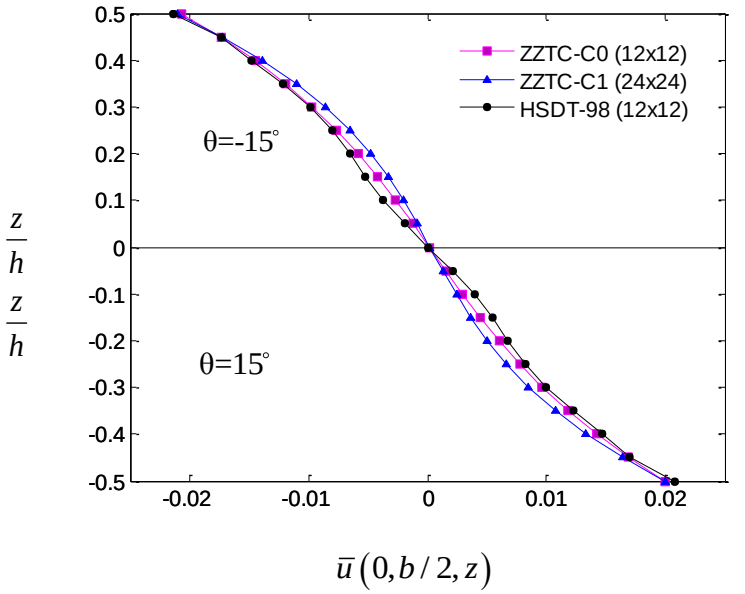

Fig. 10 Distribution of in-plane displacement through thickness of two-layer [$15^\circ/-15^\circ$] plate (a/h=4)

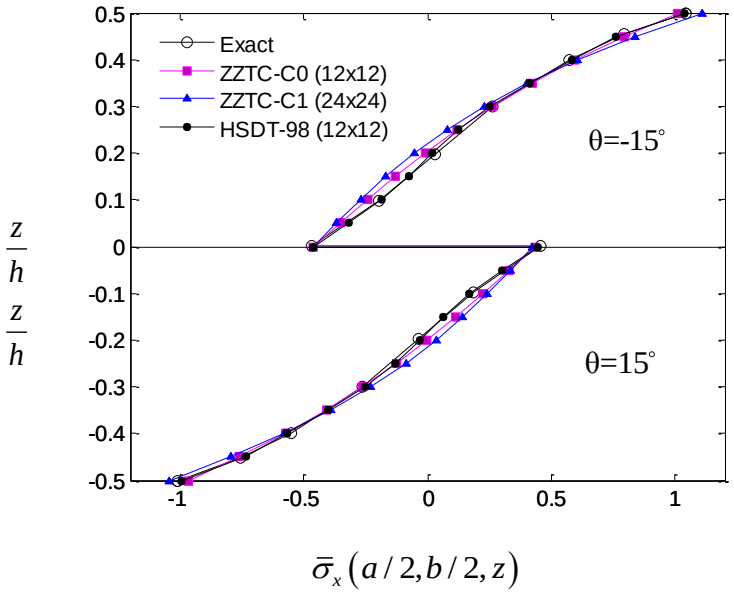

Fig. 11 Distribution of in-plane stress through thickness of two-layer [15°/-15°] plate (*a*/*h*=4)

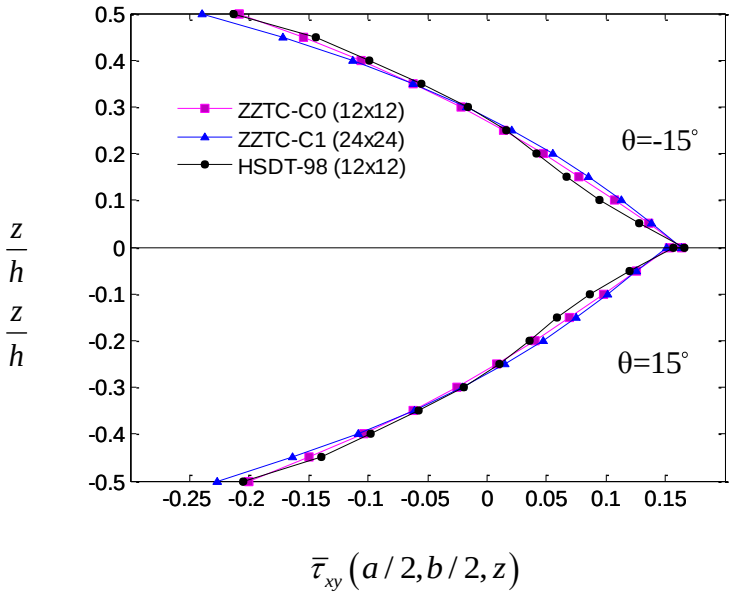

Fig. 12 Distribution of in-plane stress through thickness of two-layer [15°/-15°] plate (*a*/*h*=4)

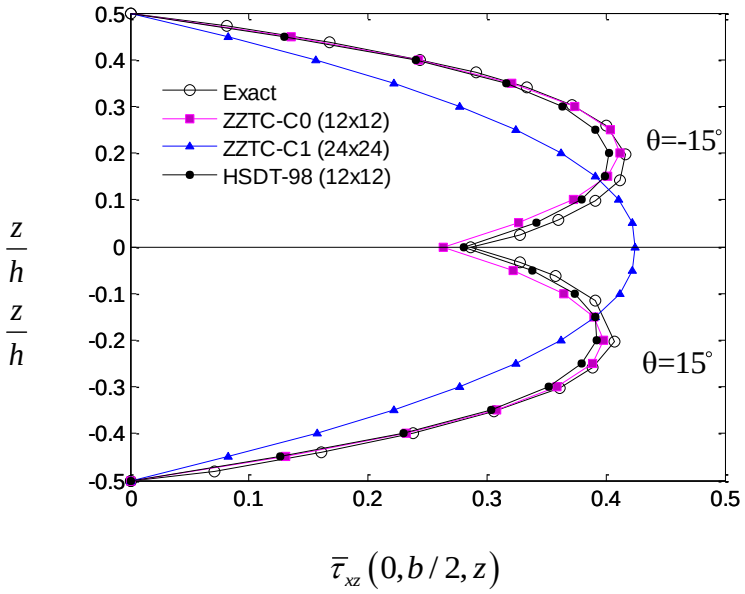

Fig. 13 Distribution of transverse shear stress through thickness of two-layer [15°/-15°] plate (a/h=4)

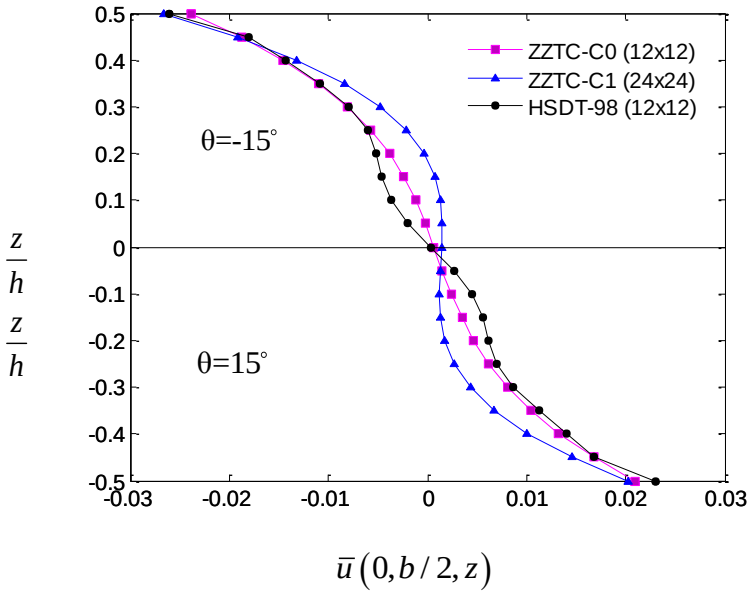

Fig. 14 Distribution of in-plane displacement through thickness of two-layer [15°/-15°] plate (a/h=2.5)

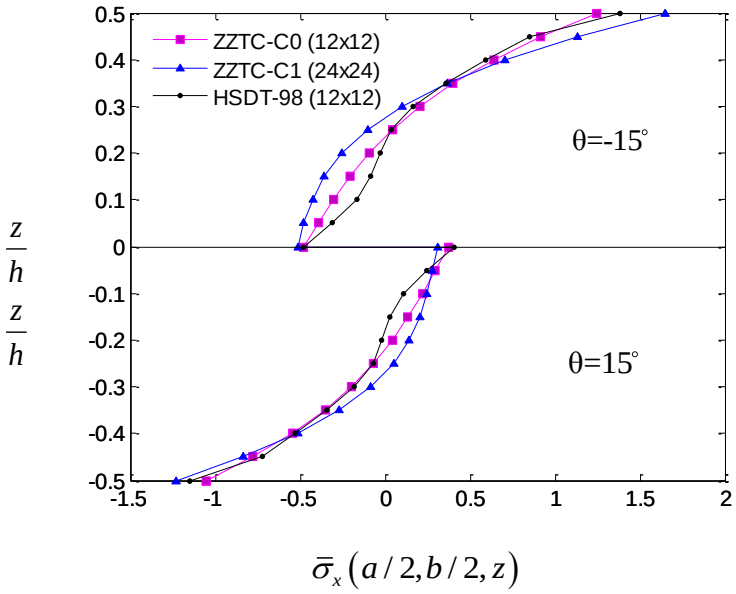

Fig. 15 Distribution of in-plane stress through thickness of two-layer [15°/-15°] plate (a/h=2.5)

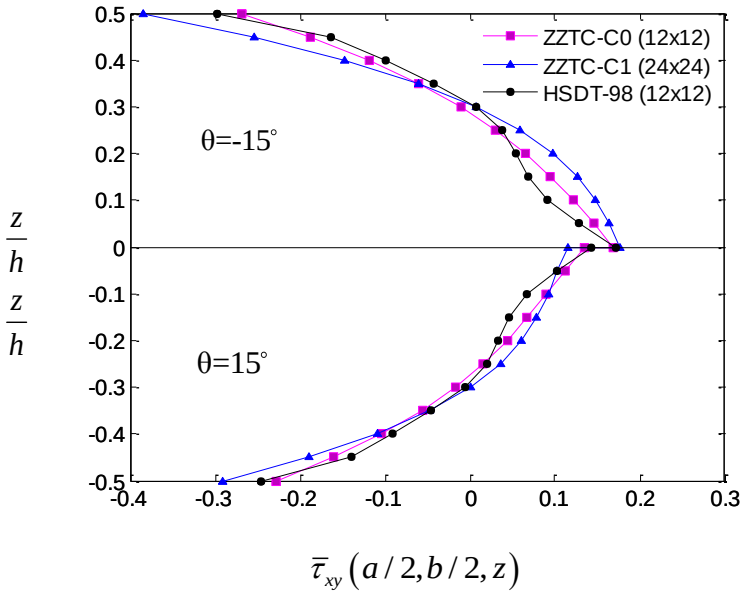

Fig. 16 Distribution of in-plane stress through thickness of two-layer [15°/-15°] plate (a/h=2.5)

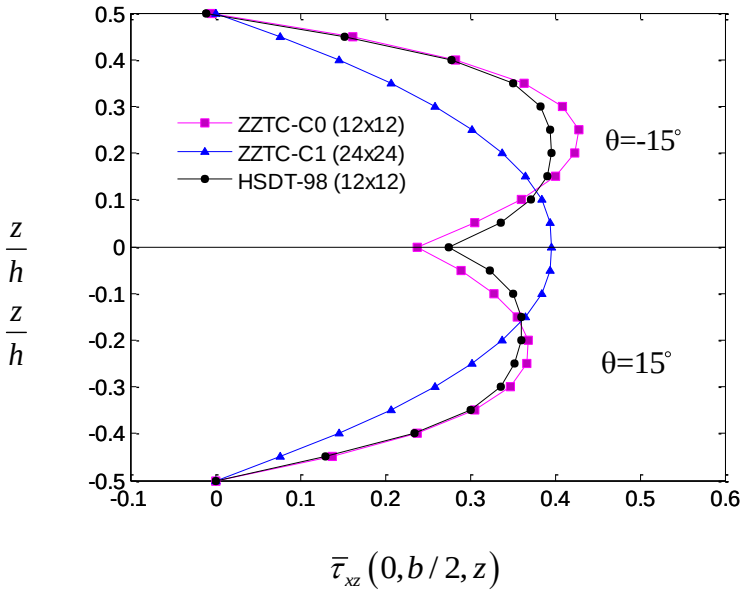

Fig. 17 Distribution of transverse shear stress through thickness of two-layer [15°/-15°] plate (a/h=2.5)

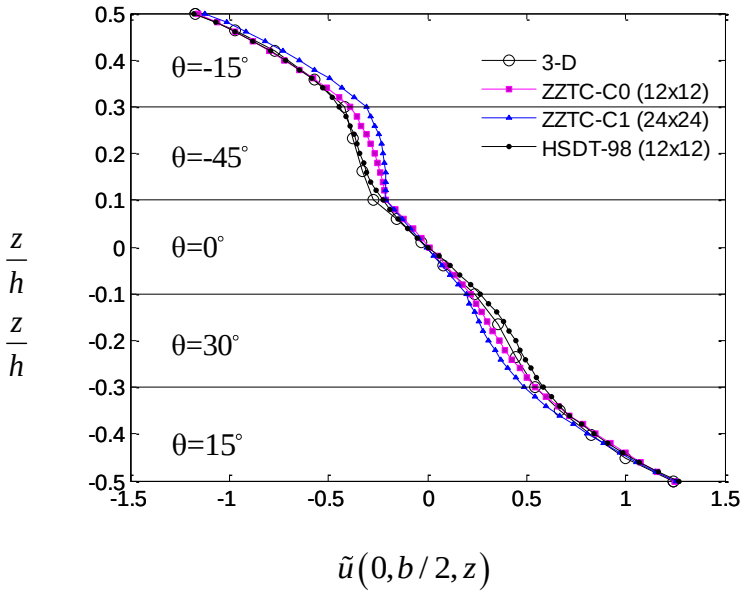

Fig. 18 Distribution of in-plane displacement through thickness of five-layer [15°/30°/0°/-45°/-15°] plate (a/h=4)

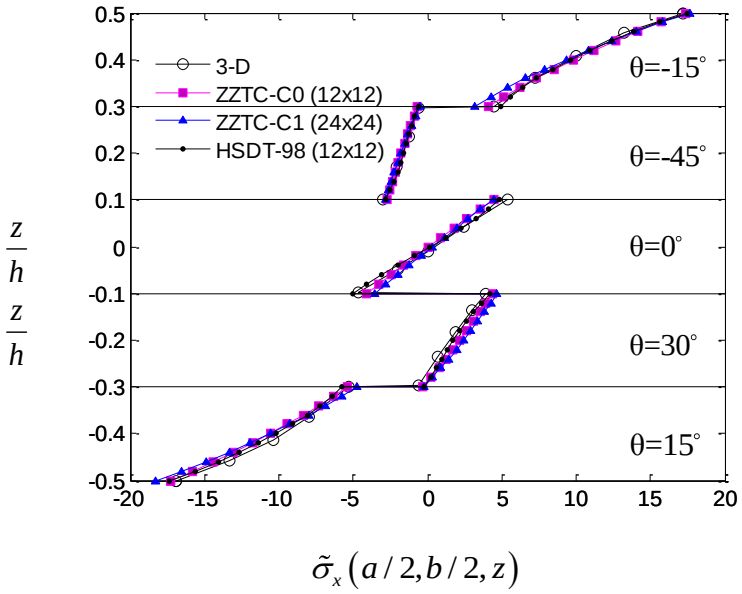

Fig. 19 Distribution of in-plane stress through thickness of five-layer $[15^\circ/30^\circ/0^\circ/-45^\circ/-15^\circ]$ plate (a/h=4)

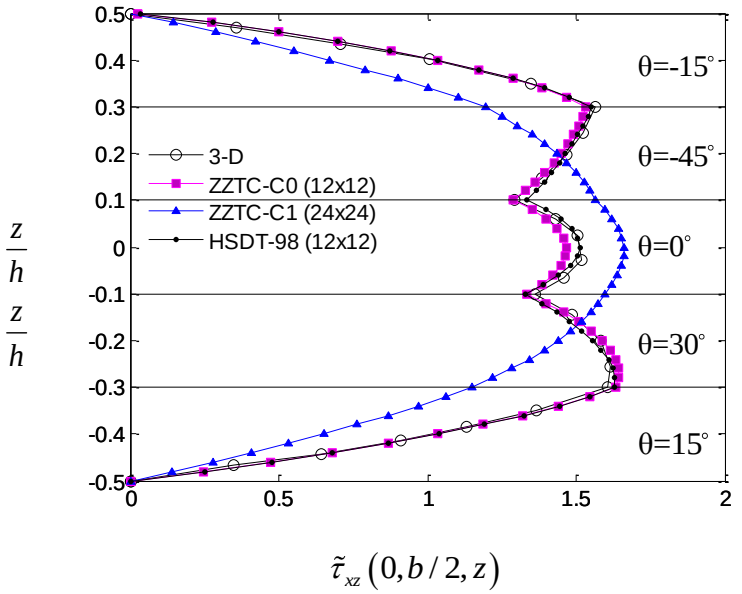

Fig. 20 Distribution of transverse shear stress through thickness of five-layer $[15^\circ/30^\circ/0^\circ/-45^\circ/-15^\circ]$ plate (a/h=4)

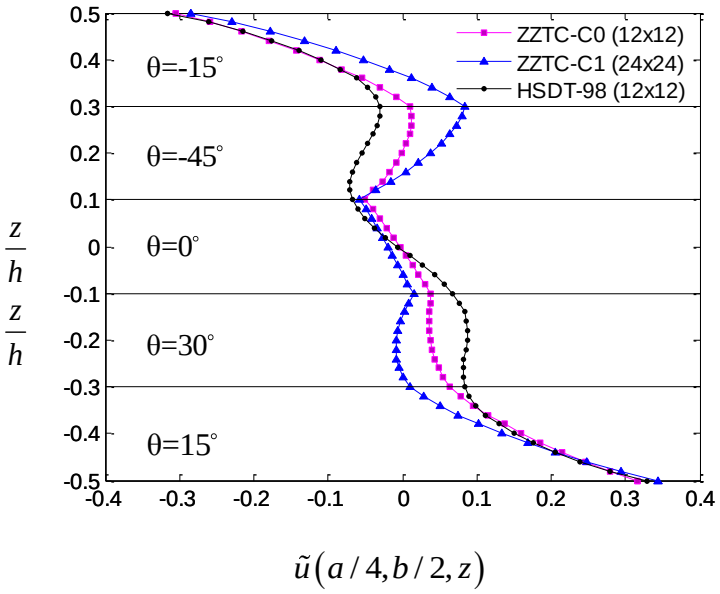

$\tilde{u}\left(a/4, b/2, z\right)$

Fig. 21 Distribution of in-plane displacement through thickness of five-layer $[15^\circ/30^\circ/0^\circ/\text{-}45^\circ/\text{-}15^\circ]$ clamped plate (a/h=4)

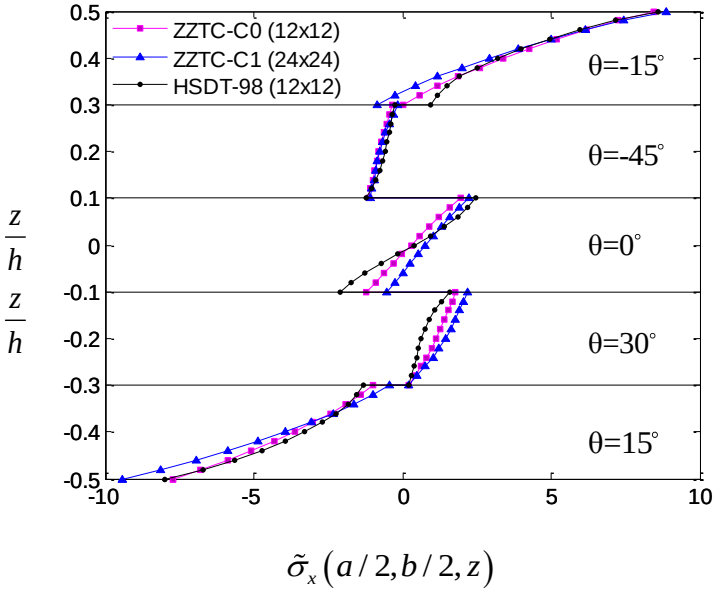

$\tilde{\sigma}_x\left(a/2, b/2, z\right)$

Fig. 22 Distribution of in-plane stress through thickness of five-layer $[15^\circ/30^\circ/0^\circ/\text{-}45^\circ/\text{-}15^\circ]$ clamped plate (a/h=4)

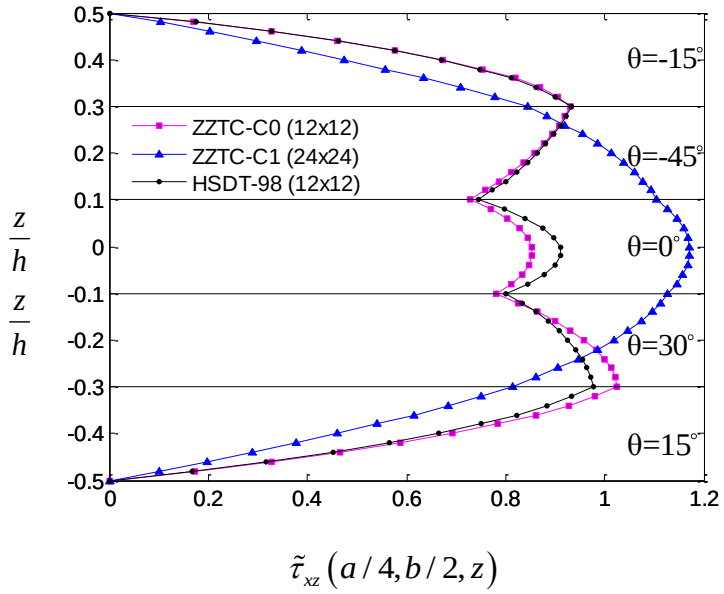

$\tilde{\tau}_{xz}\left(a/4, b/2, z\right)$

Fig. 23 Distribution of transverse shear stress through thickness of five-layer

$[15^\circ/30^\circ/0^\circ/-45^\circ/-15^\circ]$ clamped plate (a/h=4)

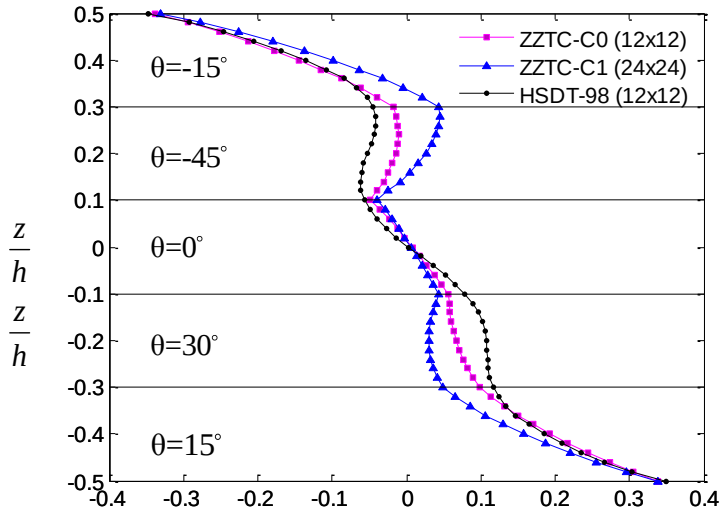

$\tilde{u}\left(0, b/2, z\right)$

Fig. 24 Distribution of in-plane displacement through thickness of five-layer

$[15^\circ/30^\circ/0^\circ/-45^\circ/-15^\circ]$ plate (a/h=2.5)

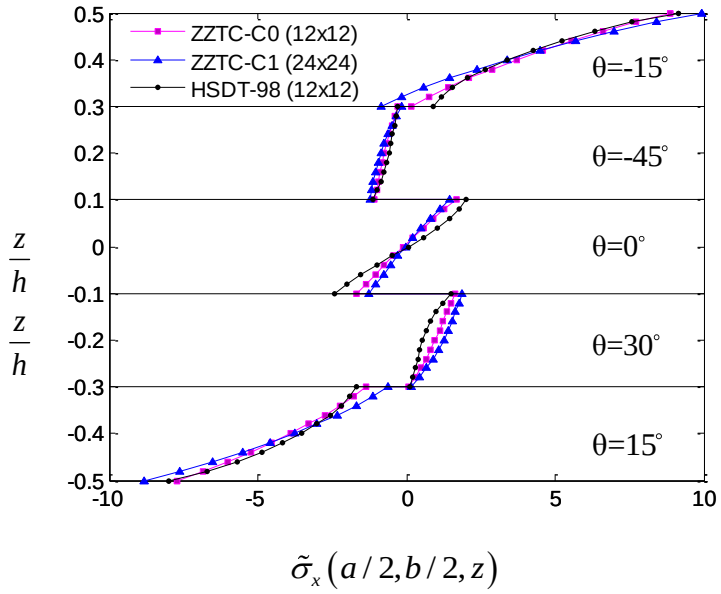

Fig. 25 Distribution of in-plane stress through thickness of five-layer $[15^\circ/30^\circ/0^\circ/-45^\circ/-15^\circ]$ plate (a/h=2.5)

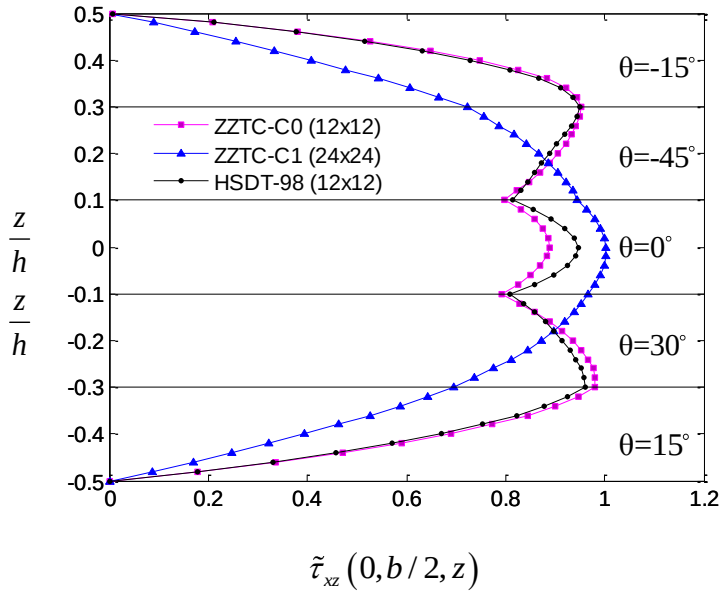

Fig. 26 Distribution of transverse shear stress through thickness of five-layer $[15^\circ/30^\circ/0^\circ/-45^\circ/-15^\circ]$ plate (a/h=2.5)

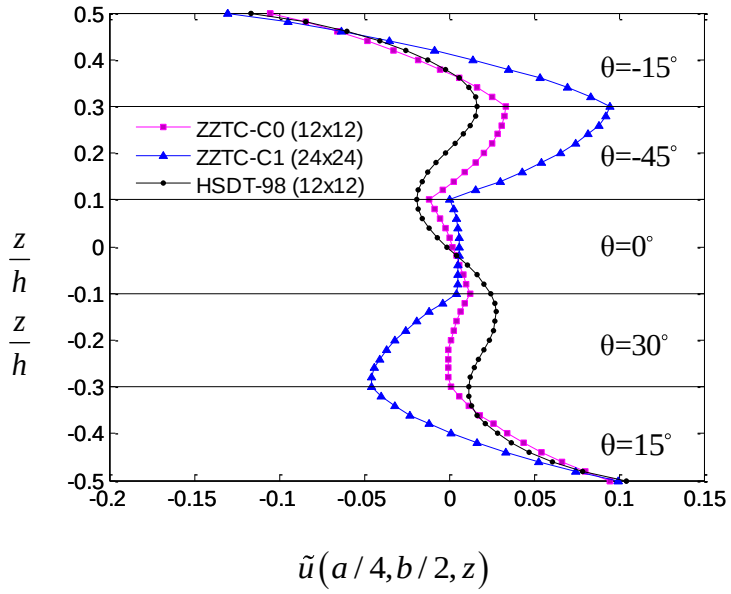

Fig. 27 Distribution of in-plane displacement through thickness of five-layer $[15^\circ/30^\circ/0^\circ/-45^\circ/-15^\circ]$ clamped plate (a/h=2.5)

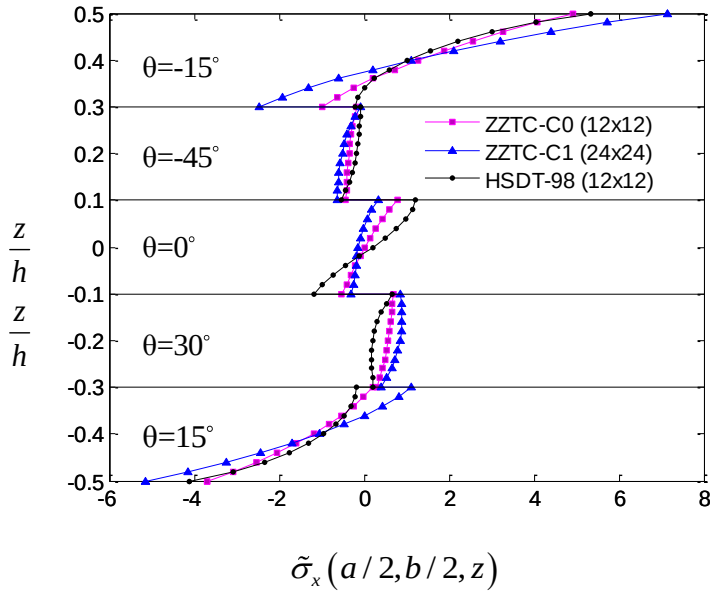

Fig. 28 Distribution of in-plane stress through thickness of five-layer $[15^\circ/30^\circ/0^\circ/-45^\circ/-15^\circ]$ clamped plate (a/h=2.5)

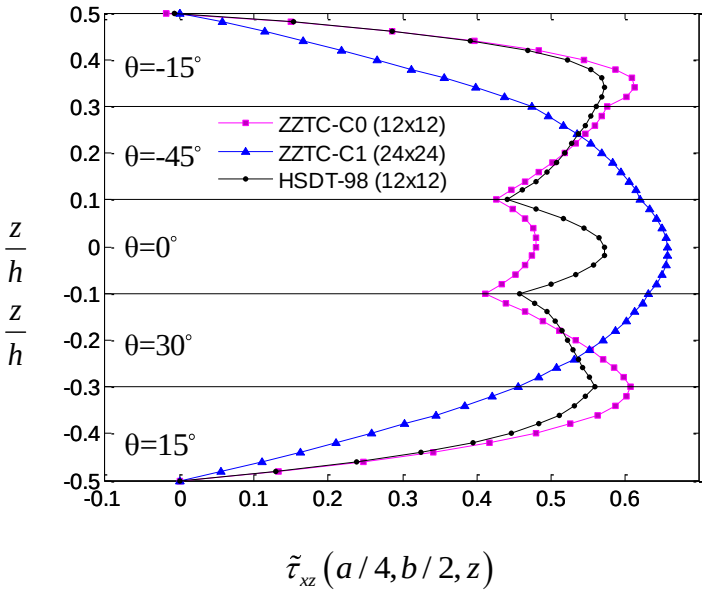

$\tilde{\tau}_{xz}\left(a/4, b/2, z\right)$

Fig. 29 Distribution of transverse shear stress through thickness of five-layer $[15^\circ/30^\circ/0^\circ/-45^\circ/-15^\circ]$ clamped plate (a/h=2.5)

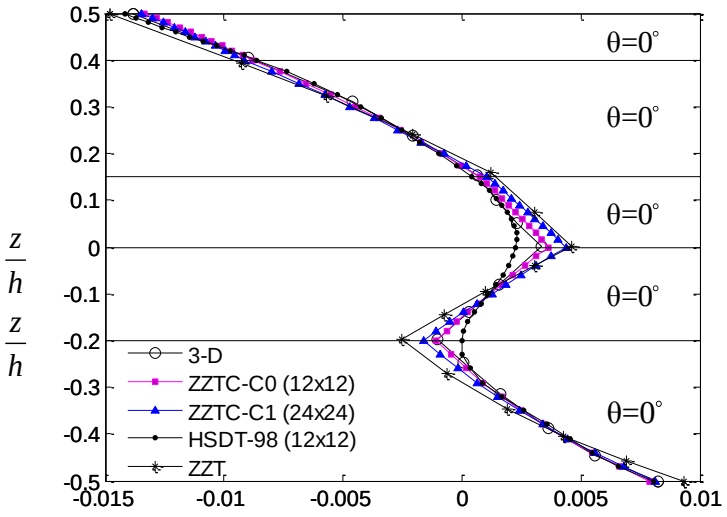

$\bar{u}\left(0, b/2, z\right)$

Fig. 30 Distribution of in-plane displacement through thickness of five-layer plate (a/h=4)

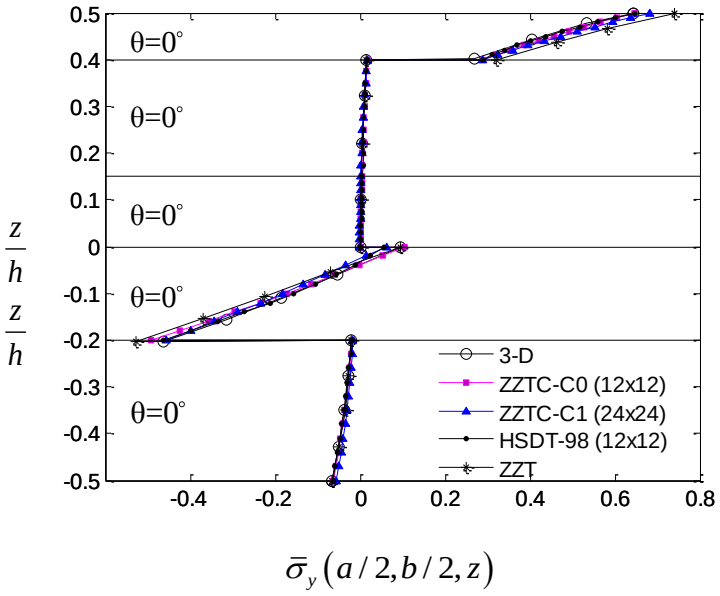

$$\bar{\sigma}_y\left(a/2, b/2, z\right)$$

Fig. 31 Distribution of in-plane stress through thickness of five-layer plate (a/h=4)

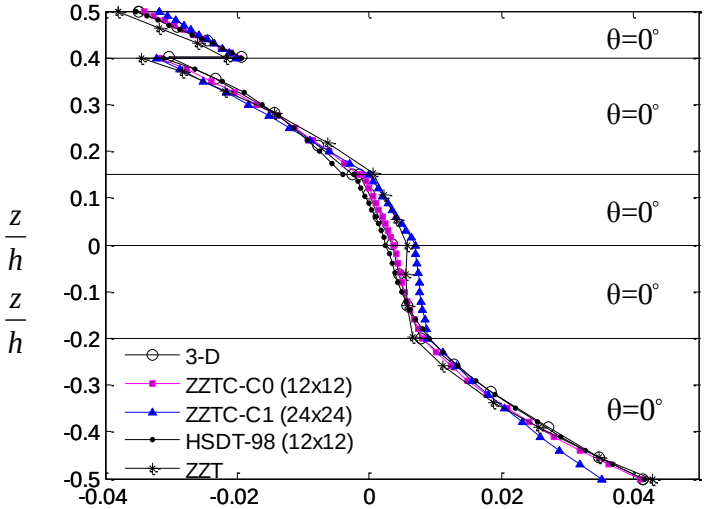

$$\bar{\tau}_{xy}\left(a/2, b/2, z\right)$$

Fig. 32 Distribution of in-plane stress through thickness of five-layer plate (a/h=4)

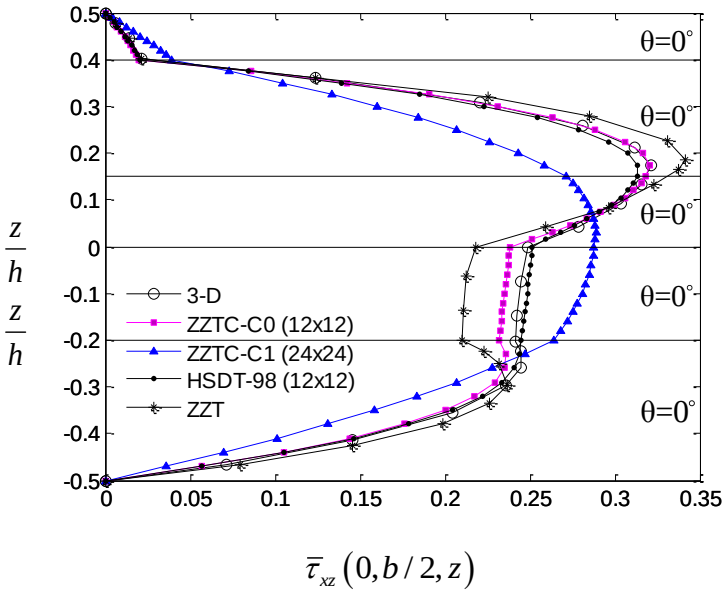

Fig. 33 Distribution of transverse shear stress through thickness of five-layer plate (a/h=4)

Tab. 1 Transverse displacement and in-plane stresses of a simply supported thin composite plate ($0^\circ/90^\circ/0^\circ$) under double sinusoidal loading

a/h		$\bar{w}$	$\bar{\sigma}_x$	$\bar{\sigma}_y$	$\bar{\tau}_{xy}$
		(a /2,a/2,0)	(a /2,a/2,h/2)	(a /2,a/2, h /6)	(0,0, h /2)
100	ZZTC-C0 (24×24)	0.4293	0.5369	0.1801	0.0213
	Exact [35]	0.4368	0.539	0.181	0.0213
200	ZZTC-C0 (24×24)	0.4261	0.5352	0.1783	0.0213
500	ZZTC-C0 (24×24)	0.4223	0.5304	0.1762	0.0216
1000	ZZTC-C0 (24×24)	0.4142	0.5196	0.1726	0.0220
	CLPT [38]	0.43125	0.53870	0.17957	0.02128

Tab. 2 In-plane stress $\bar{\sigma}_x\left(a/2, b/2, z\right)$ for a two-ply [15°/-15°] plate.

z/h	3-D [40]	Exact [38]	ZZTC-C0 (12×12)	ZZTC-C1 (24×24)	HSDT-98 (12×12)
-0.5	-0.9960	-0.9966	-0.9607 (3.60)	-1.0284 (3.19)	-0.9860 (1.06)
0^-	0.4526	0.4529	0.4336 (4.26)	0.4261 (5.91)	0.4402 (2.80)
0^+	-0.4719	-0.4716	-0.4566 (3.18)	-0.4589 (2.69)	-0.4591 (2.65)
0.5	1.0446	1.0439	1.0102 (3.23)	1.0999 (5.36)	1.0393 (0.44)

The number in bracket () is the % errors of various theories relative to exact solutions

Tab. 3 Transverse shear stress $\bar{\tau}_{xz}\left(0, b/2, z\right)$ for a two-ply [15°/-15°] plate.

z/*h*	3-D [40]	Exact [38]	ZZTC-C0 (12×12)	ZZTC-C1 (24×24)	HSDT-98 (12×12)
-0.5	0.0004	0.0000	0.0000 (0.00)	0.0000 (0.000)	0.0000 (0.00)
-0.2	0.4061	0.4066	0.3865 (4.94)	0.3447 (15.22)	0.3879 (4.59)
0^{-}	0.2887	0.2884	0.2626 (8.95)	0.4037 (39.97)	0.2841 (1.49)
0^{+}	0.2883	0.2884	0.2626 (8.95)	0.4037 (39.97)	0.2841 (1.49)
0.2	0.4183	0.4166	0.4013 (3.67)	0.3444 (17.33)	0.3945 (5.30)
0.5	0.0008	0.0000	0.0000 (0.00)	0.0000 (0.000)	0.0000 (0.00)

The number in bracket () is the % errors of various theories relative to exact solutions